Cloud Cover and Structural Observation Gaps in African Agricultural Earth Observation: Evidence from Six Agroecological Zones

Olaoye Anthony Somide
CropSense AI Research, CipherSense AI
olaoye.somide@ciphersense.ai
September 2026

The manuscript begins on the following page.

Cloud Cover and Structural Observation Gaps in African Agricultural Earth Observation: Evidence from Six Agroecological Zones

Olaoye Anthony Somide
CropSense AI Research · CipherSense AI
olaoye.somide@ciphersense.ai

September 2026

Abstract

Optical Earth observation underpins a growing number of agricultural-monitoring and agri-fintech services across Africa, all of which need a usable view of a field often enough to track its condition. Cloud gaps in that record are usually treated as random missing data; we test whether they are instead *structurally* biased. Using three growing seasons (2022–2024) of Sentinel-2 scene-classification data over cropland in six administrative zones, one per African sub-region and together spanning the climate gradient from hyper-arid to humid-equatorial, we measure the weekly frequency with which each zone's cropland yields a usable optical observation (a pixel passing the Sentinel-2 quality mask). This ranges from 55% over humid Central Africa to 81% over the arid Nile Delta; "blind-spot weeks", when more than half a zone's cropland is unobservable, run from 12% to 42%. Within every zone, usable-observation frequency falls as weekly rainfall rises (Spearman ρ from -0.34 to -0.70, $p < 0.001$ after adjusting for temporal autocorrelation); this is the study's one firmly powered result, and it reappears in an independent MODIS cloud product. With only six spatial units, the cross-regional climate gradient and the concentration of the deficit in the rain-fed growing season are reported as indicative patterns consistent with that rainfall mechanism, not as powered tests; Nile-irrigated Egypt inverts, as the mechanism predicts. Optical blind spots in African agricultural monitoring track rainfall and fall hardest on the humid, smallholder, rain-fed systems during their growing season, which motivates evaluating SAR-optical fusion for those zones. The study measures the gap, not the benefit of any fix.

Keywords

Sentinel-2, cloud cover, agricultural monitoring, Earth observation, Africa, smallholder agriculture, optical remote sensing, SAR fusion, observation bias

1. Introduction

1.1 Optical monitoring and the cloud-gap assumption

Free, analysis-ready optical imagery from the Copernicus Sentinel-2 mission has made continental-scale agricultural monitoring feasible for organisations that could never have afforded commercial tasking. Across Africa this now supports crop-type and cropland mapping, within-season vegetation-condition tracking, drought and food-security early warning, smallholder yield estimation, and the observation triggers behind parametric crop insurance. All of these products share a hidden dependency: they need a usable (cloud-, shadow- and haze-free enough) view of the same ground repeatedly through the season. When that view is lost, the pixel is simply missing, and pipelines handle it with compositing, gap-filling, or interpolation.

The near-universal working assumption is that this missingness, while inconvenient, is *unbiased*: that over enough revisits the gaps average out and every field is eventually seen. If that assumption is wrong, so that the gap is larger and more persistent in particular climates, cropping systems, or phenological windows, then optical-only monitoring is not merely noisier in those settings; it is *less accurate there by construction*, and the error is correlated with exactly the variables (humidity, smallholder density, rain-fed dependence) that describe agricultural vulnerability.

1.2 What is known, and the gap

That tropical and equatorial regions are cloudier than arid ones is not in question, and the consequences of growing-season cloud cover for passive optical monitoring have been described in general terms [4], [6]. What has not been done, to our knowledge, is a direct, multi-year, cross-regional measurement of usable optical observation frequency *over African cropland specifically*, at a resolution fine enough to connect it to the crop calendar, with the regional comparison and the hypotheses specified in advance. Continental agricultural-EO reviews for Africa identify data availability as a limiting factor [7] but do not quantify how that limit varies across the continent's climate zones or across the season. This paper provides that measurement.

1.3 Contributions

1. **A pre-specified, cross-regional measurement.** We quantify weekly usable Sentinel-2 optical observation frequency over cropland for six administrative zones spanning North, West, East, Central, and Southern Africa, across the three growing seasons 2022–2024. The zones, study period, unit of analysis, and hypotheses were written into a project document before any data were analysed (see Section 4.3); the design was not lodged with a public registry, so we use "pre-specified" rather than "pre-registered".
2. **One robust relationship and two suggestive patterns.** The relationship internal to a single location, weekly usable-observation frequency versus weekly rainfall, is negative in every zone and survives adjustment for temporal autocorrelation. Consistent with it, a cross-regional climate gradient and a concentration of the deficit in the rain-fed

growing season are both present but, at six spatial sampling units and with the growing season as one seasonal block per zone-year, are supported descriptively rather than by a powered test.

3. **Analysis at the right unit.** We separate what can be tested within a zone (the rainfall coupling) from what requires the zone or region as the unit (the gradient, the growing-season concentration), and report the latter at the zone and zone-year level with permutation and autocorrelation-aware tests, so a reader can see which numbers are load-bearing.
4. **A concrete design implication** for African agri-EO platforms: optical blind spots track rainfall and therefore fall in the rain-fed growing season, in the humid smallholder regions (the when and where that matter for monitoring), which points to radar fusion, not better optical compositing, as the direction worth evaluating.

The Sentinel-2 acquisition pipeline is not released; the derived weekly series and the analysis code are, and the method is described here in enough detail to reproduce the study independently.

2. Related Work

Cloud cover and optical monitoring. Whitcraft et al. [4], [5] established, for the GEOGLAM global agricultural-monitoring initiative, that useful optical observation opportunity varies strongly by region and month, and that parts of the tropics receive too few clear looks per month for reliable passive monitoring. Sudmanns et al. [6] characterised global Sentinel-2 clear-observation availability and found pronounced latitudinal and seasonal structure. Our work narrows this to African cropland, extends it to three seasons, and couples it to rainfall and the crop calendar rather than the calendar month alone.

Agricultural EO for Africa. Continental crop mapping and monitoring efforts [7], [8] repeatedly identify persistent cloud cover, especially over the humid, smallholder-dominated zones of Central and West Africa, as a first-order obstacle, and increasingly turn to synthetic-aperture radar (SAR) or SAR-optical fusion [9], [10] to see through it. That literature motivates fusion on general feasibility grounds; we quantify the size and the structure of the gap it is meant to close.

Scene classification. We rely on the Sentinel-2 Level-2A Scene Classification Layer produced by Sen2Cor [2]. Continuous cloud-probability approaches such as *s2cloudless* [3] are an alternative; we use the categorical layer because it is the signal available in the analysis-ready cloud-optimised archive without per-scene reprocessing, and we test sensitivity to the classification threshold directly (Section 6.1).

3. Data

3.1 Study zones

The unit of comparison is one administrative level-1 (ADM1) zone per African sub-region, six in total (two in West Africa), each representing a distinct agro-ecological setting (Table 1). Each zone was selected

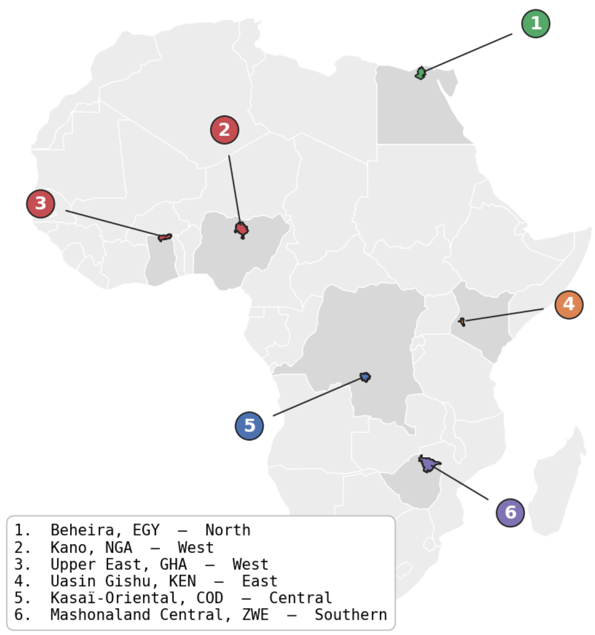

Figure 1: The six study zones. One administrative level-1 (ADM1) zone per African sub-region, coloured by region and numbered as in Table 1. Grey shading marks the six host countries. Zones were fixed before analysis and chosen to span the continental climate gradient from the arid Nile Delta to the humid Congo basin.

before any data were processed, verified to exist in the geoBoundaries ADM1 layer [13], and checked to be of broadly comparable area to the others so that a single unusually large zone could not average out its own local cloud variability. Figure 1 shows their locations and Table 1 lists them. The zones deliberately span the continental climate gradient, from the hyper-arid, fully irrigated Nile Delta to the humid forest–agriculture mosaic of south-central DR Congo, and span farming systems from mechanised irrigated agriculture to rain-fed smallholder cassava and maize.

3.2 Sentinel-2 scene classification

We use Sentinel-2 [1] Level-2A surface-reflectance products, accessed as cloud-optimised GeoTIFFs through the Element 84 Earth Search STAC catalogue (the `sentinel-2-l2a` collection). For each zone we retrieve every scene intersecting that zone's ADM1 polygon between 1 January 2022 and 31 December 2024, subject only to a coarse pre-filter removing scenes with catalogue cloud cover $\geq 95\%$ and scenes flagged with more than 5% degraded MSI data. The 95% cut is applied at the scene level; Section 6.5 bounds its effect on the cropland-level measurement and shows it raises no zone's mean by more than 1.3 points. Critically, we do **not** apply a low-cloud acceptance filter of the kind operational monitoring pipelines use to guarantee usable imagery: every scene passing the coarse pre-filter is retained and classified, because discarding high-cloud scenes by their cloud outcome would bias the very quantity we measure toward 100% by construction. The retrieval returns 8,986 scenes across the six zones over the three years.

The only per-pixel cloud signal in these products is the

Table 1: Study zones. Area from geoBoundaries ADM1; cropland fraction from ESA WorldCover class 40 on the 20 m grid; scenes = Sentinel-2 L2A items retrieved 2022–2024 after the coarse pre-filter.

Region	Country / ADM1 zone	Area (km^2)	Climate / system	Cropland	Scenes
North	Egypt / Beheira	9,826	arid, Nile-irrigated	47.6%	1,277
West	Nigeria / Kano	20,131	Sahel, rain-fed smallholder	71.0%	1,979
West	Ghana / Upper East	8,842	Guinea savanna, rain-fed smallholder	39.7%	1,423
East	Kenya / Uasin Gishu	2,955	highland, rain-fed maize	50.4%	644
Central	DR Congo / Kasaï-Oriental	17,300	humid forest–agriculture, smallholder	2.3%	680
Southern	Zimbabwe / Mashonaland Central	28,193	subtropical, smallholder maize/tobacco	18.8%	2,983

20 m Scene Classification Layer (SCL), a categorical band assigning each pixel to one of twelve classes (vegetation, bare soil, water, cloud shadow, cloud medium probability, cloud high probability, thin cirrus, and so on). No continuous cloud-probability band is present in this archive.

3.3 Rainfall

Weekly rainfall per zone is taken from CHIRPS v2.0 [11], the Climate Hazards Group InfraRed Precipitation with Station data product, aggregated from daily 0.05° rasters to a zonal weekly total and mean over the same ISO weeks as the Sentinel-2 series. The two series share the (zone, ISO-year, ISO-week) key exactly, giving 936 matched zone-weeks (six zones × 156 weeks).

3.4 Cropland mask and crop calendar

Analysis is restricted to cropland pixels using the 2021 ESA WorldCover 10 m map (v200) [12] (class 40, cropland), resampled to the 20 m SCL grid. The cropland fraction of each ADM1 zone varies by more than an order of magnitude (Table 1), from 71% for Kano to 2.3% for Kasaï-Oriental; masking keeps the reported observation frequency about the farmland that actually exists rather than diluting it with cities, forest, and bare land. Cropland pixels are interleaved with non-cropland at fine spatial scale across the full extent of every zone rather than being clustered in a sub-region, so masking changes the denominator but not the spatial coverage of the analysis.

Crop calendars are taken from FAO crop-calendar records (FAO GIEWS country-level, with agro-ecological-zone detail where available) for maize, the most widely grown rain-fed cereal across five of the six zones. The calendars carry only sowing and harvest dates, no phenological-stage field, so we define an **estimated mid-season window** as the middle third of each zone's sow-to-harvest cycle: the standard agronomic stand-in for the water-stress-sensitive flowering and grain-fill stages, which fall between first-third vegetative growth and last-third ripening. We use "mid-season window" throughout and do not claim to have observed flowering or grain-fill directly; a product with explicit stage dates would place it more precisely (Section 9).

4. Methods

4.1 Usable-observation classification

For each Sentinel-2 scene we read the 12-class Scene Classification Layer, reproject it onto a common 20 m analysis grid clipped to the zone and masked to cropland, and classify every cropland pixel as *usable* or *not usable* for that scene. A pixel that no scene covered that week is *not observed*; SCL class 0 (no-data) is treated as not observed. Table 2 gives the complete class-to-threshold mapping for the three nested thresholds.

Table 2: Sentinel-2 Scene Classification Layer classes and their treatment under each usable-pixel threshold. • = usable, blank = not usable. The strict and moderate thresholds differ only in rows 6, 7 and 11.

SCL	class	strict	moderate	lenient
0	No data (not observed)			
1	Saturated / defective			
2	Dark-area pixels			•
3	Cloud shadow			•
4	Vegetation	•	•	•
5	Not-vegetated (bare soil)	•	•	•
6	Water		•	•
7	Unclassified		•	•
8	Cloud, medium probability			•
9	Cloud, high probability			
10	Thin cirrus			•
11	Snow / ice		•	•

The **moderate** threshold is the headline. It excludes exactly the classes that indicate the surface was *not seen through a clear atmosphere* (no-data, saturated/defective, dark-area, cloud shadow, medium- and high-probability cloud, and thin cirrus), which is a common invalid-pixel set for Sentinel-2 analysis-ready workflows. Under this threshold, **water, unclassified, and snow/ice count as usable**: those pixels were observed, just not as vegetation or bare soil, and the quantity we measure is whether the surface was seen, not whether a vegetation index is computable from it. Dark-area pixels (class 2) are excluded because Sen2Cor's classifier groups them with shadow detection; excluding them, like every other borderline choice here, biases usable-observation frequency *downward*, the conservative direction for a study measuring gaps.

The **strict** threshold restricts usable to vegetation and bare soil only; that is, it differs from moderate *only* in also excluding water, unclassified, and snow/ice. Section 6.1 shows strict and moderate agree to within 1.5 points per zone, so the treatment of those three classes does not drive any result. The **lenient** threshold keeps only no-data, saturated/defective, and high-probability cloud as unusable; Section 6.1 shows it is too permissive to be a meaningful "clear observation" definition and does not preserve the gradient.

4.2 Weekly aggregation and the usable-observation metric

Scenes are composited to ISO weeks. A cropland pixel is *observed* in a given week if any scene that week returned valid data for it, and counts as a **usable optical observation** if any scene that week classified it as passing the SCL quality mask of the chosen threshold (Section 4.1); a single such look in the week is sufficient. Weekly **usable-observation frequency** for a zone is the number of usable cropland pixels divided by the number of cropland pixels in the zone.

This is a proxy for a clear-sky look, not a direct cloud measurement. It inherits whatever the SCL classifier gets right or wrong: undetected cloud, haze, or aerosol can pass the mask, and cloud shadow, thin cirrus and dark-area pixels (not all of which are cloud) are excluded from it. We use "usable observation" rather than "cloud-free observation" throughout for this reason, and Section 8 lists it as a limitation.

Only ISO weeks fully contained in the study period are reported (156 per zone). Weeks in which no scene was retrieved appear as explicit 0%-usable rows rather than being dropped; Section 6 shows these are overwhelmingly total-cloud weeks, not gaps in satellite coverage.

4.3 Statistical units and independence

Weekly usable-observation frequency is a bounded, strongly left-skewed percentage, so all tests are rank-based or permutation-based. The harder question is the unit of analysis. The study has **six spatial sampling units** (one to two zones per region), and each zone is one location observed for 156 consecutive weeks. Two consequences follow.

First, the 156 weekly values within a zone are not independent replicates of that zone's region: testing a *regional* hypothesis on 936 zone-weeks is pseudoreplication [14], and the very small p-values it produces reflect the sub-sample size, not the number of independent spatial units. We therefore test the regional gradient at the **zone level** ($n = 6$; Spearman and Pearson correlation of zone mean usable-observation frequency with zone mean rainfall) and the **zone-year level** ($n = 18$; Kruskal–Wallis across regions), and additionally fit a generalised estimating equation over all zone-weeks with zone clusters and an AR(1) within-zone working correlation; the latter uses all the data but, with six clusters, is read as indicative.

Second, the weekly series is temporally autocorrelated (lag-1 autocorrelation 0.0–0.42 by zone, effective sample size 60–160). For the **within-zone** rainfall correlation, the one comparison that lives entirely inside a single spatial unit and so is not limited by the number of zones, we report a p-value with the effective sample size substituted for n, and a 95% confidence interval from a moving-block bootstrap (13-week blocks). For the **mid-season-window** comparison, the window is one contiguous ~13-week block per zone-year, so a weekly two-sample test again overstates the sample size; we test it by **circular block permutation** of the window label (per zone and pooled), and separately ask whether the mid-season window is worse than *other weeks of the same zone's wet season.*

The falsifiable null, specified before analysis, is that usable-observation frequency shows no regional, seasonal, or rainfall structure; the primary and secondary hypotheses (a regional gradient tracking climate; a deficit concentrated in the rain-fed growing season, and specifically its stress-sensitive mid-season stages; a stronger effect in smallholder-dominant zones) were fixed in the same dated project document (Section 1.3). All of the analysis is in the accompanying code.

4.4 Acquisition completeness

Every scene passing the pre-filter (Section 3.2) is classified. A failed read is retried, and an unrecoverable read raises an error rather than being skipped, because a silently dropped scene would bias usable-observation frequency downward, the opposite of the conservative direction for a study measuring observation gaps. The scene list returned by the catalogue is pinned per zone at retrieval time, so reprocessed or backfilled scenes appearing in later queries do not change the results.

5. Results

5.1 The regional gradient

Table 3 reports, for each zone, mean weekly usable-observation frequency over cropland at the moderate threshold and the share of weeks below 50% usable. Ordered by the mean, the six zones run humid Central Africa 55%, Guinea-savanna Ghana 59%, Sahel Nigeria 68%, highland Kenya 70%, subtropical Zimbabwe 71%, arid Egypt 81%, a 26-point spread between the humid forest–agriculture mosaic of Kasaï-Oriental and the irrigated Nile Delta. By region the ordering is Central 55%, West 63%, East 70%, Southern 71%, North 81%.

At the level of the six independent spatial units, this gradient is **suggestive, not significant**. Across the six zones, mean usable-observation frequency correlates negatively with mean weekly rainfall (Spearman $\rho = -0.60$, $p = 0.21$; Pearson $r = -0.77$, $p = 0.08$), with highland Kenya as the visible exception: wet, from orographic rather than convective cloud, but well observed. At the zone-year level ($n = 18$) the regional difference is significant (Kruskal–Wallis $H = 13.3$, $p = 0.01$), and a generalised estimating equation over all zone-weeks with zone clusters gives −11 points of usable-observation frequency per unit log-rainfall, but with six clusters that estimate is read as indicative. A Kruskal–Wallis on the 936 raw zone-weeks returns $p \approx 10^{-9}$; we do not report that as evidence for a regional effect, for the reason given in Section 4.3.

Figure 2 shows the full weekly series as a zone-by-week heatmap. Every zone's distribution is left-skewed: the median week is well observed everywhere (medians 65% to 96%) and it is a minority of weeks that collapse hard. Those collapses are more frequent and deeper in the humid zones: 42% of all weeks fall below 50% usable in Kasaï-Oriental, against 12% in Beheira. This "blind-spot week" rate follows the same ordering as the mean (Table 3) and is the more decision-relevant framing for a monitoring service.

Table 3: Per-zone results, moderate threshold, 2022–2024 ($n = 156$ weeks per zone). Blind-spot weeks = weeks with $< 50\%$ of cropland usable. Rain ρ = Spearman correlation of weekly usable-observation frequency with weekly rainfall, with the p-value adjusted for temporal autocorrelation (all < 0.001). Season deficit = mean usable-observation frequency outside minus inside the estimated mid-season window (middle third of the sow-to-harvest calendar, Section 3.4; negative = window better observed); p from circular block permutation of the window label.

Zone (region)	Mean usable	Blind-spot wks	Rain ρ	Season deficit	Perm. p
Kasaï-Oriental (Central)	55.4%	42.3%	−0.51	10.0 pt	0.53
Upper East (West)	59.0%	39.7%	−0.70	38.6 pt	0.26
Kano (West)	67.6%	27.6%	−0.68	23.8 pt	0.34
Uasin Gishu (East)	69.6%	24.4%	−0.34	22.2 pt	0.007
Mashonaland C. (Southern)	71.1%	27.6%	−0.65	18.8 pt	0.44
Beheira (North)	81.4%	12.2%	−0.41	−14.9 pt	0.20
Pooled	**67.4%**	**29.0%**	—	**14.0 pt**	**0.03**

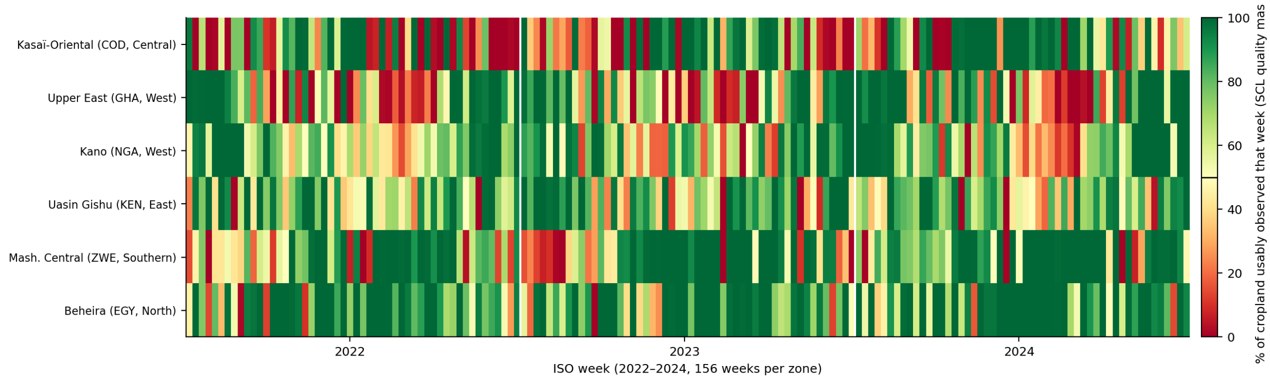

Figure 2: Weekly usable Sentinel-2 optical observation of cropland, moderate threshold, one row per zone, ordered humid to arid. Each cell is one ISO week; green = most cropland passed the SCL quality mask that week, red = little or none. White verticals mark year boundaries. The humid zones (top) collapse to red far more often and more deeply than the arid Nile Delta (bottom).

5.2 Rainfall coupling

This is the relationship that lives inside a single spatial unit, and it is the study's most solid quantitative result. Within every zone, weekly usable-observation frequency is negatively correlated with weekly rainfall (Figure 3, Table 3): more rain, more cloud, fewer usable pixels. Spearman ρ ranges from -0.70 (Upper East) to -0.34 (Uasin Gishu). After substituting the effective sample size for the temporal autocorrelation (Section 4.3), every zone's correlation is significant at $p < 0.001$, and a moving-block bootstrap 95% confidence interval excludes zero in every zone (the tightest is Uasin Gishu at $[-0.46, -0.24]$, the widest Kasaï-Oriental at $[-0.64, -0.34]$). Egypt's rank correlation (-0.41) is real even though its Pearson correlation is not significant, because almost every week there has near-zero rainfall. Lagged correlations (rainfall one or two weeks earlier against usable-observation frequency now) are weaker than the same-week correlation in every zone but one, so the dominant effect is same-week cloud during rain, not multi-week cloud persistence after a rain event.

5.3 The growing-season and mid-season window

For rain-fed agriculture the rainfall coupling has a direct operational reading: the deficit falls in the growing season, when the crop is on the ground. Overlaying each zone's maize calendar, weeks inside the estimated mid-season window (Section 3.4) are observed at 55.5% usable on average against 69.5% for the rest of the year, a 14-point deficit, and the blind-spot rate rises from 27% to 41% (Figure 4). Descriptively this is the sharpest expression of the pattern.

Its statistical support is weaker than the raw comparison suggests, because the window is a single contiguous ~13-week block per zone-year rather than ~140 independent weeks. Tested by circular block permutation of the window label (Section 4.3), the pooled deficit is only marginally significant ($p = 0.03$) and individually significant in one of the six zones (Kenya, $p = 0.007$). Restricting the comparison to the wettest 40% of each zone's weeks, the window is not reliably worse than other wet-season weeks in four of the five rain-fed zones. The honest statement is that the deficit is a **rainy-season** effect that, for rain-fed crops, coincides with the crop's mid-season stages; whether it is *sharper* inside the mid-season window than across the wet season generally is not established at this sample (Sections 8, 9).

Egypt is the informative exception. Its mid-season weeks are *better* observed than the rest of the year (94% vs 79%). The estimated window is the wettest part of the year in the five rain-fed zones, confirming the calendar mapping tracks each zone's rainy season, but in Egypt the July–September maize window has essentially zero rainfall: Beheira's agriculture is Nile-irrigated, so its crop calendar is decoupled from rainfall and therefore from the mechanism this paper describes. The growing-season deficit is conditional on rain-fed agriculture, which is the smallholder-dominant

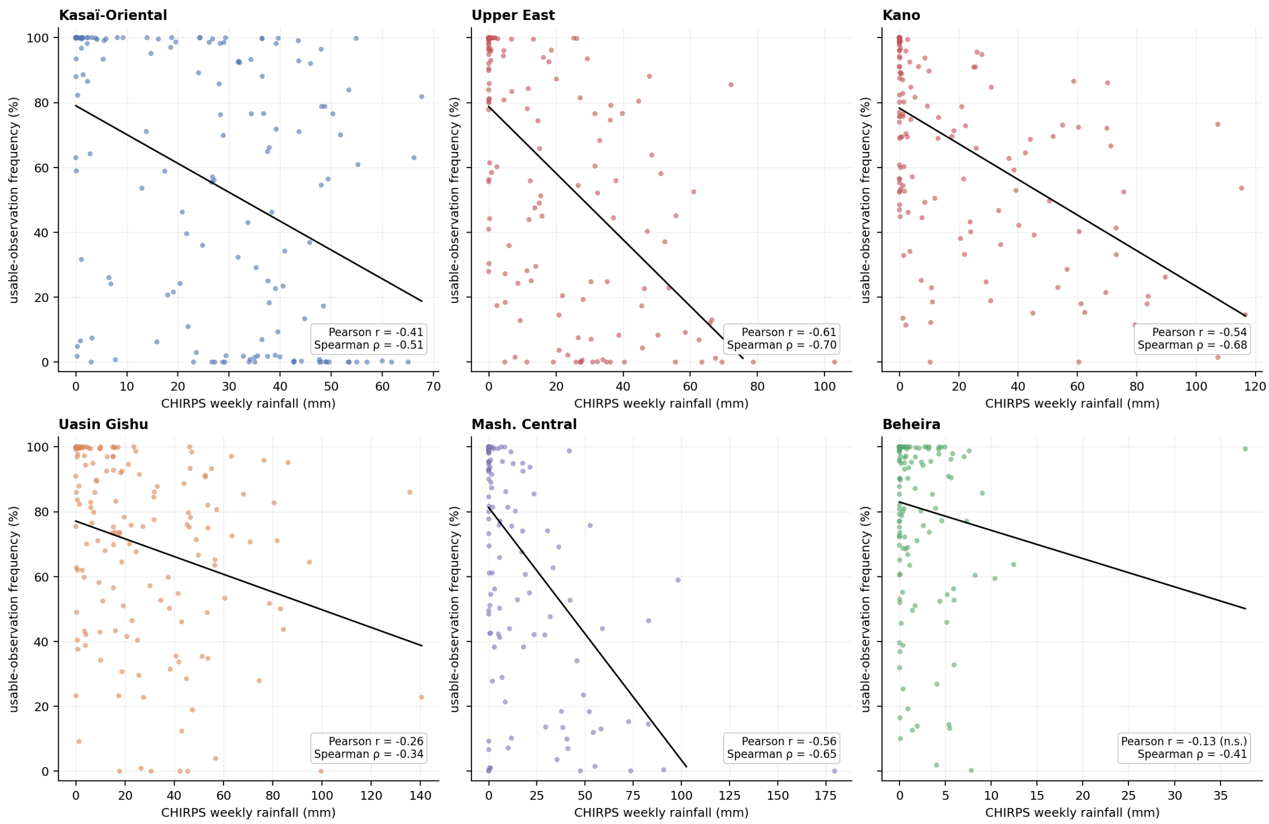

Figure 3: Weekly rainfall versus usable-observation frequency, one panel per zone. CHIRPS weekly rainfall on the x-axis, weekly usable-observation frequency on the y. This comparison is internal to a single zone. The relationship is negative in every zone (Spearman ρ inset) and stays significant at $p < 0.001$ after adjusting for temporal autocorrelation; Beheira's near-zero rainfall in most weeks flattens its linear fit.

setting where monitoring is hardest to do any other way.

5.4 Zero-observation weeks

Fifteen of the 936 zone-weeks returned no scene at all under the coarse cloud pre-filter, which makes them ambiguous between "no acquisition" and "every scene $\geq$ 95% cloud." Re-querying those weeks without the filter resolves it. Thirteen of the fifteen are total-cloud weeks: scenes existed, but the least-cloudy scene was 96–100% clouded, several at 100%. All ten such weeks in Kasaï-Oriental are total cloud. Only two weeks (both in Uasin Gishu) are genuine acquisition gaps, and excluding them moves East Africa's mean by under one point. Counting total-cloud weeks as 0% usable is correct; they are the strongest instances of the effect measured here, not an artifact.

6. Robustness

6.1 Sensitivity to the usable-pixel threshold

The strict threshold differs from moderate only in also excluding water, unclassified, and snow/ice pixels (Table 2). Moving between the two changes each zone's mean by 0.3 to 1.5 points, in the same direction for every zone, so it is a level shift rather than a reordering: the six-zone ordering is identical and monotonic from humid to arid under both, the humid-to-arid spread is 26–27 points, and the zone-level rainfall correlation is unchanged (Spearman $\rho \approx -0.6$). Thirty-one of the 936 zone-weeks have a strict/moderate gap above 5 points (flood weeks in highland Uasin Gishu, wet-season weeks in Kasaï-Oriental), but they are too few to move the zone means. The **lenient** threshold does break the pattern: counting cloud-medium-probability and thin-cirrus pixels as usable compresses every zone to 72–89%, collapses the between-zone spread, and makes the ordering non-monotonic. We therefore report the gradient as holding under the strict and moderate definitions and not under a deliberately permissive one. The within-zone rainfall correlation is negative and significant in every zone at all three thresholds; the growing-season deficit is present in direction at all three but, as in Section 5.3, marginal.

6.2 Sensitivity to the choice of year

Recomputing per year, the full six-zone rank ordering is not reproduced in any single year: East and Southern Africa differ by about one point over the full period and swap between 2022–23 and 2024, and Kasaï-Oriental climbs steeply enough (48%, then 53%, then 65%) to overtake West Africa in 2024. What is stable every year is the ends of the gradient (Central Africa worst or second-worst, North Africa best) and the within-zone rainfall correlations, which stay negative in every zone in every year. Kasaï-Oriental's upward trend is a genuine climate signal, not an acquisition or processing artifact: 2022 was its wettest year and 2024 its driest in the CHIRPS record, its count of total-cloud weeks fell from seven to zero over the three years, and acquisition density was essentially flat (+11%).

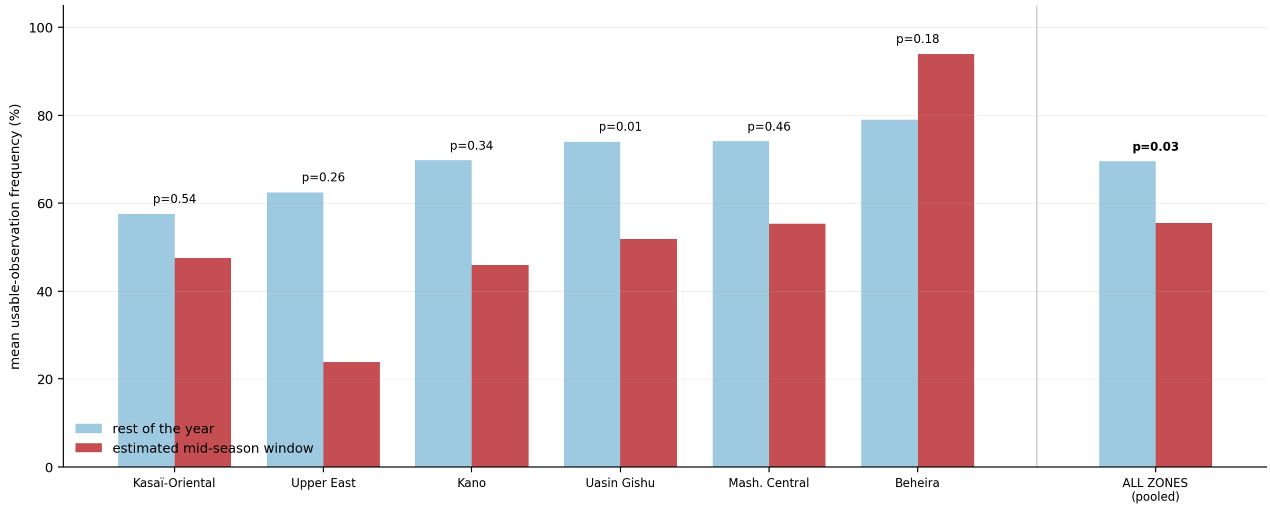

Figure 4: Usable-observation frequency inside the estimated mid-season window versus the rest of the year. The window is the middle third of each zone's sow-to-harvest calendar, an approximation of the maize flowering/grain-fill period (Section 3.4), not an observed crop stage. Blue = rest of year, red = window. p is from a circular block permutation of the window label (Section 4.3), which respects the fact that the window is one contiguous seasonal block per zone-year: the ~14-point pooled deficit is descriptively clear but only marginally significant ($p = 0.03$), and individually significant in one of six zones. Nile-irrigated Beheira inverts, as the rainfall mechanism predicts.

6.3 Sensitivity to the cropland mask

Re-running the entire study over the full ADM1 polygons instead of cropland only shifts each zone's mean by at most 2.3 points (Kasaï-Oriental, whose 2.3% cropland is marginally better observed than its surrounding forest); every other zone moves by less than 1.1 points. The six-zone ordering is identical, the zone-level rainfall correlation is unchanged, and the Kasaï-Oriental year trend persists. (The unmasked run has far more pixels per zone, but not more independent spatial units, so it does not add statistical power for the regional comparison, only confidence that the cropland mask is not the source of the pattern.)

6.4 What does not hold

The pre-specified secondary hypothesis, that within West Africa the Sahel zone (Kano) is worse observed than the Guinea-savanna zone (Upper East), is **not** supported: the zone means differ by 8.6 points in the expected direction on two zones over three years, which is a difference of one zone-pair, not a test. More broadly, at six spatial sampling units neither the within-region contrast nor the cross-regional gradient is resolvable as a powered significance test; both are reported descriptively (Section 5.1), and the load-bearing inferential result is the within-zone rainfall coupling.

6.5 Sensitivity to the scene-level cloud pre-filter

The coarse `eo:cloud_cover < 95` filter (Section 3.2) acts on the whole scene, not on the cropland within the zone, so a mostly-clouded scene could in principle still carry a clear view of the farmland. We bound its effect without re-reading pixels. Querying the catalogue for the complement of the filter (every scene at $\geq$ 95% scene cloud cover) returns 1,350 such scenes, dropped from between 14 and 98 of each zone's 156 weeks. The weekly usable-observation metric is monotonic in the number of scenes, so restoring them can only raise it, and a dropped scene at cloud cover c adds at most $(100 - c)$ points of usable cropland. Applying that bound to the least-cloudy dropped scene in every affected week, and assuming (contrary to the scattered layout of cropland in these zones, Section 3.4) that its entire clear fraction falls on cropland, each zone's mean rises by **at most 1.3 points** (Kano; the other five by 1.2 or less): Kasaï-Oriental, the zone the concern targets, moves from 55.4% to no more than 56.4%. The six-zone ordering is unchanged and blind-spot-week rates move by at most 1.4 points. No single zone-week could change by more than five points even under this deliberately generous bound, so there is no ambiguous subset left to resolve with a direct read.

A direct check points the same way. On the nine weeks that had exactly one retained scene (where the weekly usable-observation frequency *is* that scene's over-cropland usable fraction), the over-cropland value averages 8.8 points *below* 100 − (scene cloud cover), not above it. A mostly-clouded scene is, if anything, cloudier still over the cropland, the opposite of the concern.

6.6 Cross-check against an independent cloud product

Because the metric is an SCL-mask pass rate, it inherits Sen2Cor's classification behaviour. We cross-check it against MCD06COSP [15], the combined Terra and Aqua MODIS daily cloud-mask fraction on a 1° grid: a different instrument (MODIS, not the Sentinel-2 MSI) and a different algorithm. For each of the 936 zone-weeks we take MODIS clear-sky fraction as $100 \times (1 - \text{daytime cloud-mask fraction})$ and compare it to the SCL usable-observation frequency.

The two series agree on structure and differ only in level. MODIS reproduces the six-zone humid-to-arid ordering exactly (Spearman $\rho = 1.0$ on the zone means). The within-zone rainfall coupling replicates in every zone and is if anything sharper in MODIS (Spearman ρ from

−0.62 to −0.91, against −0.34 to −0.83 for SCL; all significant after the Section 4.3 autocorrelation adjustment). The growing-season deficit is present in MODIS too (pooled 15 points against 14), with the same Egypt inversion. The two differ in a systematic offset (SCL usable-observation frequency runs 10 to 24 points above MODIS clear-sky fraction) that follows from the definitions: a pixel is usably observed if *any* scene that week caught it clear, whereas the MODIS figure is a time-averaged instantaneous fraction. It does not affect this paper's within-zone and rank-based comparisons. At 1° the MODIS grid is coarse for the smaller zones (Section 8), so this checks the pattern, not the absolute values.

7. Discussion

7.1 The gap is structured, not random

One relationship is on firm ground and two patterns point the same way. The firm one: within every zone, usable-observation frequency falls as rainfall rises, it survives the temporal-autocorrelation and block-bootstrap corrections, and it reappears in an independent MODIS cloud product (Section 6.6). Pointing the same way, but resting on only six spatial units: the humid zones are worse observed than the arid ones (a 26-point spread between the extremes), and the deficit is concentrated in the rain-fed growing season. Because rainfall *is* the growing season for rain-fed agriculture, these are not really independent findings: they are the same rainfall effect seen at the regional and the seasonal scale. Read together they say optical missingness in African agricultural monitoring is not random with respect to agricultural risk: it is heaviest over the humid, smallholder, rain-fed systems, during the months the crop is in the field. A monitoring product that treats cloud gaps as ignorable will be least reliable in those places and months, and its errors will be spatially and temporally correlated rather than averaging out. What we cannot yet claim from six zones is that any *region* differs from another as a formal matter, or that the deficit is sharper in the estimated mid-season window than across the wet season generally.

7.2 Implications for agri-EO platform design

For a platform serving African agriculture, the practical consequence is that optical-only pipelines have a structural ceiling that better compositing cannot lift: in a zone with 42% blind-spot weeks, no amount of cloud-masking recovers a view that was never acquired. Sentinel-1 C-band SAR, which is unaffected by cloud, has an overlapping revisit and is available in the same open archive; SAR-optical fusion for crop condition and classification is an active field [9], [10]. Our contribution to that design question is to show the gap is not only large but tracks rainfall, so any benefit from fusion would be concentrated: it would matter most in exactly the humid, high-blind-spot, smallholder zones, and in the growing-season months, that a purely optical accuracy audit would already flag as a platform's least reliable regions and periods.

7.3 Correlation, not yet consequence

This study establishes a structural observation pattern. It does not measure the downstream effect on the accuracy of a specific yield model, condition index, or insurance trigger, nor its financial incidence on farmers, nor whether SAR or SAR-optical fusion in fact closes the gap it identifies; those are follow-on work (Section 9). The claim here is bounded: the input data to African agri-EO is systematically thinner in predictable places and times, and that is a reason to evaluate radar fusion, not yet evidence that fusion is the fix.

8. Limitations

Six spatial sampling units. This is the binding limitation. With one to two zones per region, the regional gradient and the growing-season concentration cannot be tested as formal effects; they are reported descriptively and at the zone / zone-year level (Sections 4.3, 5.1, 5.3). A denser zone sample, tens of zones, is what a powered regional test needs, and it is the first item of future work.

Repeated measures. The 156 weekly values per zone are temporally autocorrelated, so any test that treats them as independent overstates its significance. We handle this with effective sample sizes, moving-block bootstraps, and circular block permutation, but these are corrections to an imperfect design, not substitutes for more independent units.

What "usable" measures. The metric is a cropland pixel passing the SCL quality mask, which is a proxy for a clear-sky look rather than a direct cloud measurement. It inherits Sen2Cor's classification errors in both directions (undetected cloud, haze and aerosol can pass the mask, and cloud shadow, thin cirrus and dark-area pixels that are not cloud are excluded), and it says nothing about atmospheric-correction quality on the pixels that do pass. The three-threshold sensitivity analysis (Section 6.1) partially bounds this, and an independent MODIS cloud product (Section 6.6) reproduces the cross-zone ordering and the rainfall coupling from a different instrument and a different algorithm; a systematic level offset between the two is explained by the metric definitions.

Mid-season window is a calendar approximation. The window is a calendar third (Section 3.4), not an observed stage: we did not measure flowering or grain-fill. It assumes a fixed cycle shape and ignores planting-date spread and year-to-year shifts. The rainfall cross-check (Section 5.3) at least confirms it lands in the wettest part of each rain-fed zone's year; Section 9 covers what would sharpen it.

One crop. The growing-season analysis is maize-specific. Other staples (cassava, sorghum, rice) have different calendars and different stress physiology.

Kasaï-Oriental's small denominator. At 2.3% cropland the lowest-observed zone has the fewest cropland pixels and the highest week-to-week variance; the unmasked re-run (Section 6.3) is the main defence, and its zone mean moves only 2.3 points.

9. Future work

The measurement here is descriptive; four directions would turn it into something a monitoring platform can act on.

From observation gap to product error. The natural next study couples the weekly usable-observation series to a specific downstream product (a yield model, an NDVI-based condition index, an index-insurance trigger) and quantifies how much accuracy and timeliness that product loses in the high-blind-spot zones relative to the well-observed ones, and where in the season the loss falls. This converts a structural pattern into a measured cost and is the basis for any claim about financial incidence on farmers.

Measuring what SAR recovers. This paper motivates Sentinel-1 SAR fusion but does not measure its benefit. Repeating the analysis with C-band SAR added would test the recommendation directly and size the fusion payoff per zone. The questions are which zone-weeks radar makes observable that optical alone does not, and how that varies by region and by season. Such an analysis has to account for SAR's own constraints, including speckle, a less direct crop-condition signal, incidence-angle effects, and its own acquisition geometry.

More spatial units. Six zones cannot power a regional test (Section 8). Extending the same pipeline to a dense sample of ADM1 zones (tens per region) or to a continental grid would make "region" a properly replicated factor, produce a blind-spot-rate map of African cropland, show whether the climate gradient is smooth or has thresholds, and let the bias be related quantitatively to smallholder density and food-insecurity indicators. It would also give the zone-years needed to test whether the deficit is genuinely sharper inside the mid-season window than across the wet season; that test also needs stage-resolved phenology (a land-surface-phenology product or ESA WorldCereal seasonality, reconciled against the calendars) in place of the calendar third.

Predicting blind-spot weeks. Because the deficit tracks same-week rainfall and the crop calendar, both known or forecastable in advance, a platform could predict which zone-weeks will be blind spots and preemptively schedule SAR or commercial optical tasking for them, rather than discovering the gap after the fact.

The MODIS cross-check (Section 6.6) could be extended with a higher-resolution product (Landsat cloud fraction, or a reanalysis cloud field) to test the small zones at their own scale rather than at 1°.

10. Conclusion

Across three growing seasons and six zones spanning the African climate gradient, usable Sentinel-2 optical observation of cropland is not evenly hard to obtain. Within every zone it is harder when it rains; this relationship holds after correcting for the temporal autocorrelation of the weekly series, reappears in an independent MODIS cloud product, and is the study's one firmly supported inferential result. The humid zones are worse observed than the arid ones (a 26-point spread between the extremes) and the deficit is concentrated in the rain-fed growing season; with six spatial sampling units these are reported as descriptive patterns consistent with the rainfall mechanism, not as powered regional or seasonal tests, and a denser zone sample is needed to establish them formally. The one irrigated zone inverts the seasonal pattern, as the rainfall mechanism predicts. Taken together the picture is that optical blind spots in African agricultural monitoring track rainfall, and so fall hardest on the humid, smallholder, rain-fed systems during the months the crop is in the field, the places and periods a monitoring platform most needs to see. For platforms building on optical EO across the continent, that is a strong motivation to evaluate radar fusion, targeted at the humid smallholder zones and the growing season; this study sizes the gap, and whether fusion closes it is the next test.

Acknowledgements

Sentinel-2 data courtesy of the EU Copernicus programme; CHIRPS courtesy of the Climate Hazards Center, UC Santa Barbara; land cover courtesy of ESA WorldCover; crop calendars courtesy of FAO GIEWS; MODIS MCD06COSP courtesy of NASA and the LAADS DAAC. Analysis used the Element 84 Earth Search STAC API and the AWS Open Data `sentinel-cogs` archive.

References

[1] M. Drusch et al., "Sentinel-2: ESA's optical high-resolution mission for GMES operational services," *Remote Sens. Environ.*, vol. 120, pp. 25–36, 2012, doi: 10.1016/j.rse.2011.11.026.

[2] M. Main-Knorn, B. Pflug, J. Louis, V. Debaecker, U. Müller-Wilm, and F. Gascon, "Sen2Cor for Sentinel-2," in *Proc. SPIE 10427, Image and Signal Processing for Remote Sensing XXIII*, 2017, art. 1042704, doi: 10.1117/12.2278218.

[3] A. Zupanc, "Improving cloud detection with machine learning," Sentinel Hub Blog, Sinergise, 2017, describing the s2cloudless algorithm. [Online]. Available: medium.com/sentinel-hub/improving-cloud-detection-with-machine-learning-c09dc5d7cf13

[4] A. K. Whitcraft, E. F. Vermote, I. Becker-Reshef, and C. O. Justice, "Cloud cover throughout the agricultural growing season: Impacts on passive optical earth observations," *Remote Sens. Environ.*, vol. 156, pp. 438–447, 2015, doi: 10.1016/j.rse.2014.10.009.

[5] A. K. Whitcraft, I. Becker-Reshef, and C. O. Justice, "A framework for defining spatially explicit earth observation requirements for a global agricultural monitoring initiative (GEOGLAM)," *Remote Sens.*, vol. 7, no. 2, pp. 1461–1481, 2015, doi: 10.3390/rs70201461.

[6] M. Sudmanns, D. Tiede, H. Augustin, and S. Lang, "Assessing global Sentinel-2 coverage dynamics and data availability for operational Earth observation (EO) applications using the EO-Compass," *Int. J. Digit. Earth*, vol. 13, no. 7, pp. 768–784, 2020, doi: 10.1080/17538947.2019.1572799.

[7] C. Nakalembe and H. Kerner, "Considerations for AI-EO for agriculture in Sub-Saharan Africa," *Environ. Res. Lett.*, vol. 18, no. 4, art. 041002, 2023, doi: 10.1088/1748-9326/acc476.

[8] H. Kerner, G. Tseng, I. Becker-Reshef, C. Nakalembe, B. Barker, B. Munshell, M. Paliyam, and M. Hosseini, “Rapid response crop maps in data sparse regions,” in *Proc. KDD Workshop Humanitarian Mapping*, 2020, arXiv:2006.16866.

[9] J. Reiche, E. Hamunyela, J. Verbesselt, D. Hoekman, and M. Herold, “Improving near-real time deforestation monitoring in tropical dry forests by combining dense Sentinel-1 time series with Landsat and ALOS-2 PALSAR-2,” *Remote Sens. Environ.*, vol. 204, pp. 147–161, 2018, doi: 10.1016/j.rse.2017.10.034.

[10] K. Van Tricht, A. Gobin, S. Gilliams, and I. Piccard, “Synergistic use of radar Sentinel-1 and optical Sentinel-2 imagery for crop mapping: A case study for Belgium,” *Remote Sens.*, vol. 10, no. 10, art. 1642, 2018, doi: 10.3390/rs10101642.

[11] C. Funk et al., “The climate hazards infrared precipitation with stations—a new environmental record for monitoring extremes,” *Sci. Data*, vol. 2, art. 150066, 2015, doi: 10.1038/sdata.2015.66.

[12] D. Zanaga et al., “ESA WorldCover 10 m 2021 v200,” Zenodo, 2022, doi: 10.5281/zenodo.7254221.

[13] D. Runfola et al., “geoBoundaries: A global database of political administrative boundaries,” *PLoS ONE*, vol. 15, no. 4, art. e0231866, 2020, doi: 10.1371/journal.pone.0231866.

[14] S. H. Hurlbert, “Pseudoreplication and the design of ecological field experiments,” *Ecol. Monogr.*, vol. 54, no. 2, pp. 187–211, 1984, doi: 10.2307/1942661.

[15] R. Pincus, P. A. Hubanks, S. Platnick, K. Meyer, R. E. Holz, D. Botambekov, and C. J. Wall, “Updated observations of clouds by MODIS for global model assessment,” *Earth Syst. Sci. Data*, vol. 15, pp. 2483–2497, 2023, doi: 10.5194/essd-15-2483-2023. Data: MCD06COSP_D3_MODIS Collection 6.2, doi: 10.5067/MODIS/MCD06COSP_D3_MODIS.062.